THE ASTRONOMICAL JOURNAL VOLUME 113, NUMBER 4 APRIL 1997

THE PECULIAR MORPHOLOGY OF THE IRREGULAR GALAXY NGC 1427A

SERGIO A. CELLONE[1,2]

Facultad de Ciencias Astronómicas y Geofísicas, Universidad Nacional de La Plata, and Complejo Astronómico El Leoncito, CC 467, 5400 San Juan, Argentina
Electronic mail: cellone@castec.edu.ar

JUAN CARLOS FORTE[1]

Instituto de Astronomía y Física del Espacio, and Facultad de Ciencias Astronómicas y Geofísicas, Universidad Nacional de La Plata, CC 67, Suc. 28, 1428 Buenos Aires, Argentina
Electronic mail: forte@iafe.uba.ar

Received 1996 October 25; revised 1996 December 19

ABSTRACT

Multicolor surface photometry and fragmentary low-resolution spectroscopy of the irregular galaxy NGC 1427A are presented. This galaxy, a member of the Fornax Cluster, has not been studied in detail previously. It shows a very distinctive morphology: a low surface brightness stellar background with several bright knots forming a distorted ring-like structure. A faint plume and several diffused filaments connect the northern part of the main body of the galaxy with an object having elliptical isophotes. The overall aspect of NGC 1427A, then, resembles that of known interacting galaxies. The very blue colors of the bright knots show that they are composed by young stars, and several of them also show emission lines. The northern object, which has itself a couple of these blue knots, is bluer than the background of the main body of the galaxy. This fact indicates that the star formation histories in both objects have been different. Morphologically, the northern object is similar to the numerous dwarf elliptical or irregular galaxies that populate the Fornax Cluster. The possibility of an interaction being the cause of the particular structure of this galaxy is discussed. © *1997 American Astronomical Society.* [S0004-6256(97)00604-3]

1. INTRODUCTION

NGC 1427A is an irregular galaxy, member of the Fornax Cluster. It has been described in these words: "*It has no definite center, and its shape is vague and irregular. It contains a large number of gaseous and luminous clusters, which partially form a ring towards the western edge of the galaxy*" (Laustsen *et al.* 1987). In fact, a distinctive feature of this galaxy is the lack of any nucleus, bar, or central condensation; all its star forming regions are distributed along what seems a distorted ring.

Feitzinger & Galinski (1985) describe it as "knotty, several stars superposed," in their catalog of southern (suspected) dwarf galaxies. However, most of these "stars superposed" are in fact bright knots (H II regions or large young star complexes, i.e., the "gaseous and luminous clusters" mentioned in the preceding paragraph) belonging to this galaxy, as will be shown later (see Sec. *3.3*).

Ferguson (1989) classifies NGC 1427A as Im III. Adopting a distance modulus $m-M=31.4$ for the Fornax Cluster (Bothun *et al.* 1989; van den Bergh 1989), its observed total aparent blue magnitude ($B_T=13.4$ mag) corresponds to a total absolute magnitude $M_B=-18.0$, or one full magnitude brighter than the LMC. Hence, NGC 1427A is clearly not a "dwarf" ($M_B>-16.0$) galaxy, according to the most popular definition currently in use (Tammann 1980). Instead, it is the most luminous irregular galaxy in the Fornax Cluster.

NGC 1427A has a projected distance to NGC 1399 (the dominant elliptical galaxy in Fornax) of 22.8 arcmin, or 126 kpc, with the adopted distance. Its heliocentric radial velocity of 1973 ± 20 km s^{-1} (Jones & Jones 1980) is somewhat larger than the Fornax Cluster's mean velocity (1366 km s^{-1}; $\sigma_V=325$ km s^{-1}) (Ferguson & Sandage 1990).

H I observations (Aaronson *et al.* 1981; Reif *et al.* 1982; Bureau *et al.* 1996) give a radial velocity in agreement with optical data ($2020-2028$ km s^{-1}), and reveal a gaussian 21 cm profile, typical of irregular (i.e., pressure supported instead of rotating) systems. Its total H I mass is $M_{\rm H\,I}=8.39\times10^9 M_\odot$, i.e., higher than the median for giant Irr galaxies (Hunter & Gallagher 1985). Other global properties of NGC 1427A are comparable to the average values for giant Irr's: $M_B=-18.0$, major axis $\simeq12$ kpc, and width of the H I line at 20% of maximum $(\Delta V_{\rm H\,I})_{20}=117-150$ km s^{-1}. As a consequence, NGC 1427A has a somewhat larger than average $M_{\rm H\,I}/L_B$ ratio (see, for example, Fig. 6 in Sprayberry *et al.* 1995).

Isserstedt & Schindler (1986) use a simple photometric method for determining the ratio of present to average star formation rate (SFR) in galaxies, and they find that this ratio is higher in NGC 1427A than in most other galaxies in their

[1]Visiting Astronomer, Cerro Tololo Inter-American Observatory. CTIO is operated by AURA, Inc. under contract to the National Science Foundation.
[2]Visiting Astronomer, Complejo Astronómico El Leoncito, operated under agreement between the Consejo Nacional de Investigaciones Científicas y Técnicas de la República Argentina and the Universities of La Plata, Córdoba, and San Juan.

 0004-6256/97/113(4)/1239/11/$10.00

sample, even those named "assymmetric," which tend to have larger ratios than "symmetric" galaxies.

NGC 1427A is also detected as an *IRAS* "Faint Source" at 60 μm and 100 μm, with observed fluxes $F_{60}=0.2073$ Jy and $F_{100}=0.7782$ Jy, respectively. Computing its far-infrared (FIR) flux in the usual way (de Jong *et al.* 1984), we obtained $F_{\rm FIR}=1.847\times10^{-11}$erg cm^{-2} s^{-1}, or $\log(F_{\rm FIR})=-10.73$. With its quoted blue magnitude, we obtained $\log[L_{\rm FIR}/L_B]=-0.214$. This value is smaller than what is observed for interacting disk galaxies, but it is typical for normal disk galaxies (Kennicutt *et al.* 1987). It is also smaller compared to bright Irr's such as NGC 4449, but larger compared to fainter Irr's like DDO 47 and DDO 50 (Hunter *et al.* 1986). The 100 μm to 60 μm flux ratio is $\log(F_{100}/F_{60})=0.574$, or relatively high compared to normal disk galaxies, indicating a low color temperature of $\approx$28 K; so its FIR luminosity is rather high for this color temperature (de Jong *et al.* 1984), although well within the range spanned by normal late type galaxies (Soifer *et al.* 1987). This indicates that, whatever is the cause of the definetly not normal appearance of NGC 1427A, it has not resulted in a star formation rate as high as in strongly interacting systems.

The peculiar morphology of NGC 1427A attracted our attention during a visual inspection of plate #358 of the ESO Sky Survey, while looking for dwarf low surface brightness (LSB) galaxies (see Sec. 2). This galaxy clearly stands out against bright ellipticals and spirals, which are mostly burnt out in that plate. However, NGC 1427A should not be called a LSB galaxy, at least in the sense that its surface brightness is not different from what is normal for Irr galaxies. We calculated the mean of the average surface brightnesses for all the galaxies classified as irregulars in the *Second Reference Catalogue of Bright Galaxies* (de Vaucouleurs *et al.* 1976); since there are three sources of morphological classification in that catalog, we first considered all galaxies classified as irregulars in at least one of the sources, and then all galaxies classified as irregulars in all three sources; we obtained $\langle\overline{S_B}\rangle=14.15$ ($\sigma=0.77$) mag arcmin^{-2} in the first case (108 galaxies), and $\langle\overline{S_B}\rangle=14.53$ ($\sigma=0.89$) mag arcmin^{-2} in the second case (22 galaxies). In comparison, NGC 1427A has an average surface brightness $\langle S_B\rangle=14.13$ mag arcmin^{-2} (using B_T from Ferguson 1989 and D_{25} from de Vaucouleurs *et al.* 1976); i.e., not fainter than most irregulars (but see Sec. *3.1*).

Summarizing, despite its global properties are normal for an Irr galaxy, the following aspects make NGC 1427A an interesting object:

(1) Its peculiar morphology suggests a galaxy undergoing some kind of distortion, resembling known interacting galaxies.
(2) It is the only *bright* Irr galaxy in Fornax; all other irregulars are dwarfs with $B_T\geqslant16.3$ mag (Ferguson 1989).
(3) No detailed study of this particular galaxy has been previously made.

2. OBSERVATIONS

CCD direct images of NGC 1427A were obtained during two runs at CTIO (1989 October and 1990 November) as a complement to a program involving dwarf elliptical (dE) galaxies. The Washington system C ($\lambda_{\rm eff}=3910$ Å; $\Delta\lambda=1100$ Å), M ($\lambda_{\rm eff}=5085$ Å; $\Delta\lambda=1050$ Å), and T_1 ($\lambda_{\rm eff}=6330$ Å; $\Delta\lambda=800$ Å) filters were used. This photometric system was originally used to define color indices sensitive to metallicity variations in individual red giant stars (Canterna 1976). Later, Geisler & Forte (1990) found a good correlation between the integrated $C-T_1$ color and metallicity for some 50 galactic globular clusters. This color–metallicity calibration was used to study globular clusters associated with NGC 1399, one of the central elliptical galaxies in Fornax (Geisler & Forte 1990; Ostrov *et al.* 1993), as well as LSB dwarf galaxies in the same cluster (Cellone *et al.* 1994). Synthetic Washington colors were also derived for a number of model stellar populations spanning a range both in age and metallicity aiming at studying the stellar populations in those dwarf galaxies (Cellone & Forte 1996, hereafter CF96).

TABLE 1. Log of observations.

Filter/Grating	Number	Exposure time (sec)	Telescope	Date
C	3	1700	1.5 m CTIO	1989 October
M	4	1200	0.9 m CTIO	1990 November
T_1	3	1300	1.5 m CTIO	1989 October
316 g/mm	5	10800	2.1 m CASLEO	1994 December

The nights were photometric, and the seeing ranged from 1.5″ to 1.8″. The scale was 0.55″/pix for the C and T_1 frames, and 0.49″/pix for the M frames. Standard stars from Geisler (1990) were also observed for calibration purposes.

A low resolution optical spectrum with a 133 arcsec long slit placed at the southern edge of the galaxy was obtained with a cassegrain spectrograph at the 2.15 m telescope of the Complejo Astronómico El Leoncito (CASLEO). It spans a spectral range from 3600 Å to 6800 Å, with a dispersion of 3.4 Å per pixel. Table 1 logs the observations. Column (2) is the number of individual frames taken, while column (3) gives the total exposure time after co-adding them.

2.1 Image Handling

2.1.1 Direct imaging

The sky level was fitted by a plane and subtracted from each individual frame; for measuring the sky level, care was taken in selecting regions not affected by the outermost LSB features of the galaxy. Visual inspection of large-scale images from the Digitized Sky Survey confirms that we have reached far enough from the galaxy to measure the real sky background. Then, frames taken with the same filter were registered using field stars as a reference and shifted to the nearest pixel; bad pixels (most ones due to cosmic rays) were interactively interpolated, and finally the frames were co-added.

The three resultant images were transformed to a common reference frame. For the M image, this involved both a rota-

[3]The Image Reduction and Analysis Facility (IRAF) is distributed by the Association of Universities for Research in Astronomy, Inc., under contract to the National Science Foundation.

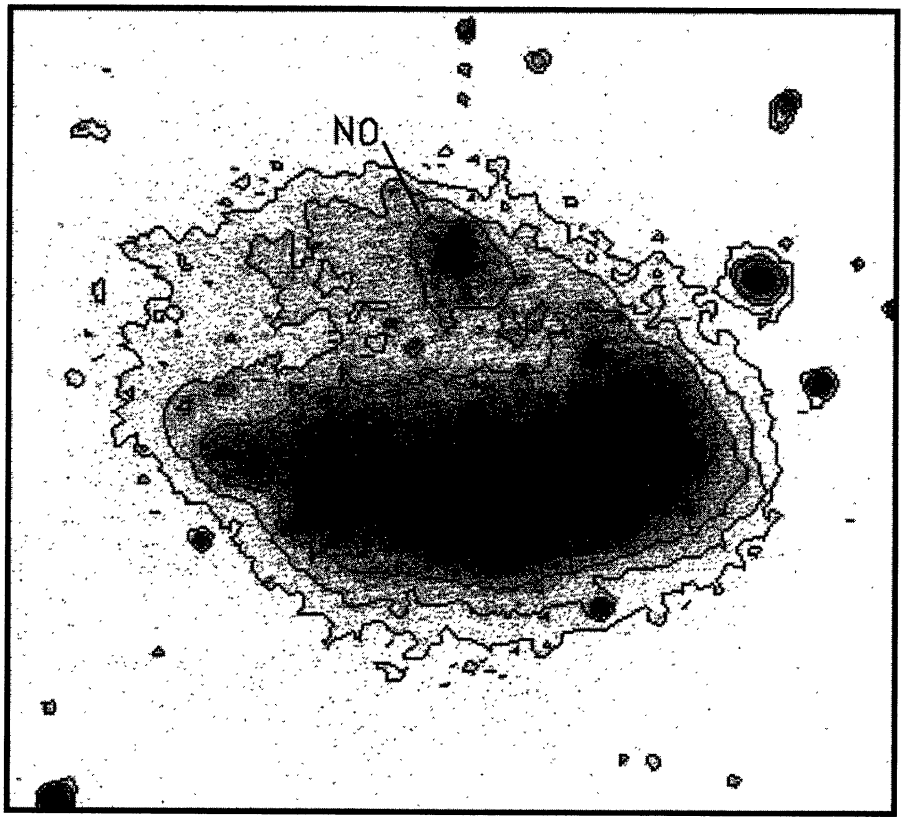

FIG. 1. *C* band image of NGC 1427A, with a greyscale contrast adjusted to show high surface brightness features. Low surface brightness isophotes, corresponding to $S_C=25.1$ mag arcsec^{-2}, $S_C=24.6$ mag arcsec^{-2}, and $S_C=24.1$ mag arcsec^{-2}, respectively, are shown as contours. They correspond to $S_B\simeq25.0$ mag arcsec^{-2}, $S_B\simeq24.5$ mag arcsec^{-2}, and $S_B\simeq24.0$ mag arcsec^{-2}, respectively (see Sec. *3.1*). The "North Object" (NO) is labeled. North is up and east to the left; the image is 200″ wide per 180″ high.

tion and an expansion since it was acquired with a different instrumental setup. Small seeing differences were eliminated by gaussian filtering the M and the T_1 frames in order to match the (higher) FWHM of the C frame.

2.1.2 Spectroscopy

Image processing was done with IRAF[3] following standard procedures. Cosmic rays were removed in a similar way as for the direct images. From the resultant two–dimensional image, three one–dimensional spectra, corresponding to the bright knots #2, #5, and #13 (see Sec. *3.3*), were extracted. These spectra were wavelength callibrated using HeNeAr comparison spectra, and flux calibrated with the spectrophotometric standard star LTT 3864 (Baldwin & Stone 1984).

3. DATA ANALYSIS AND RESULTS

3.1 Morphology and Global Properties

Figure 1 is the resultant C band image of NGC 1427A where the gray level scale has been adjusted to enhance high surface brightness (HSB) structures, while the lower surface brightness isophotes are displayed as contours. In order to show "cleaner" isophotes, the contours were drawn from a 5×5 pix median filtered image.

One can see that the irregular shape of this galaxy is not due to a chaotic distribution of recent or current star forming regions on a more symmetrically distribution of older stars (which is normal in most undisturbed Irr galaxies, e.g., Gallagher & Hunter 1984); instead, the underlying stellar distribution in NGC 1427A is quite asymmetric. Considering the region bounded by the lowest surface brightness contour in Fig. 1, there is a striking asymmetry between the south half of the galaxy, where almost all the HSB regions are concentrated, and the north half, dominated by several LSB features forming a sort of plume. Embedded within this plume there is a feature with a nearly circular shape that practically detaches from the northern edge of the main body of the galaxy. This feature, hereafter named the "North Object" (NO), has itself a few HSB regions. Several faint "wisps" can be seen pointing southwards from the NO, suggesting a connection or an interaction with the main body of the galaxy.

Regarding the HSB zones, their distribution is not completely chaotic; instead, they are arranged in a distorted ring-like shape, resembling peculiar galaxies such as Arp 125 and Arp 142 (Arp 1966). In particular, the model suggested by Freeman & de Vaucouleurs (1974) for Arp 144, the "folded ring" galaxy, closely matches the spatial distribution of the HSB zones in NGC 1427A.

Table 2 lists some global properties of NGC 1427A. Total magnitudes and colors were derived summing up all the light within the $S_C=25.1$ mag arcsec^{-2} isophote; linear dimen-

TABLE 2. Global properties.

T_1 (mag)	12.80±0.02
$C-M$ (mag)	0.25±0.04
$M-T_1$ (mag)	0.55±0.04
Major axis (kpc)	13.5
Minor axis (kpc)	9.2
B (mag)[a]	13.52±0.05
$B-V$ (mag)[a]	0.46±0.04
$\langle S_B \rangle$ (mag arcmin^{-2})[a]	14.8
M_B (mag)	−17.9
$V_{R_{(OPTICAL)}}$ (km sec^{-1}) [b]	1973±20
$V_{R_{(HI)}}$ (km sec^{-1}) [c]	2020
F_{HI} (Jy km sec^{-1}) [d]	23.1±1.2
M_{HI} ($M_\odot$)[c]	8.39×10^9
$F_{60\,\mu m}$ (Jy) [e]	0.2073
$F_{100\,\mu m}$ (Jy)[e]	0.7782

[a]Calibration from Geisler 1996.
[b]Jones & Jones 1980.
[c]Aaronson *et al.* 1981; Reif *et al.* 1982.
[d]Bureau *et al.* 1996.
[e]*IRAS* Faint Source Catalog.

sions also refer to the same isophote. Conversions to B and $B-V$ were done with the transformations given by Geisler (1996), and distance dependant quantities were derived using $m-M=31.4$, as quoted in Sec. 1.

Note that our B magnitude is consistent with Ferguson's (1989) value ($B_T=13.4$ mag), although slightly different apertures were used in both works. Our $\langle S_B \rangle$ is 0.65 mag arcmin^{-2} fainter than the value obtained in Sec. 1; however, it is within 1σ of both average values for Irr galaxies obtained from de Vaucouleurs *et al.* (1976).

3.2 Color Map

Color maps are well suited to visualize differences throughout the projected image of a galaxy. With this purpose, we made a color map of NGC 1427A; a more detailed and quantitative analysis of the colors measured in different regions of this galaxy is left for the following subsection. We used the $C-T_1$ color index because it provides the widest wavelength baseline available from our observations, and because the M frame showed a small residual of light (probably scattered light) which could not be completely corrected.

The resultant C and T_1 frames described in the preceding section were again gaussian smoothed ($\sigma=0.5$ pixels) to reduce noise, but trying to minimize any further loose of spatial resolution. Then, they were transformed to standard magnitudes, and combined to define a $C-T_1$ color map.

Sky noise usually attempts against a clear visualization of color maps. To circumvent this, we made a mask by flagging out all pixels with an intensity lower than $2\sigma_{SKY}$ in either the C or the T_1 frames and applied this mask to our $C-T_1$ map. The result is shown in Fig. 2, where darker grey levels correspond to bluer pixels; sky pixels, which should be dominated by noise, are mostly black in this figure.

Comparing this color map with Fig. 1 one immediately sees that, as expected, the bright knots are easily distin-

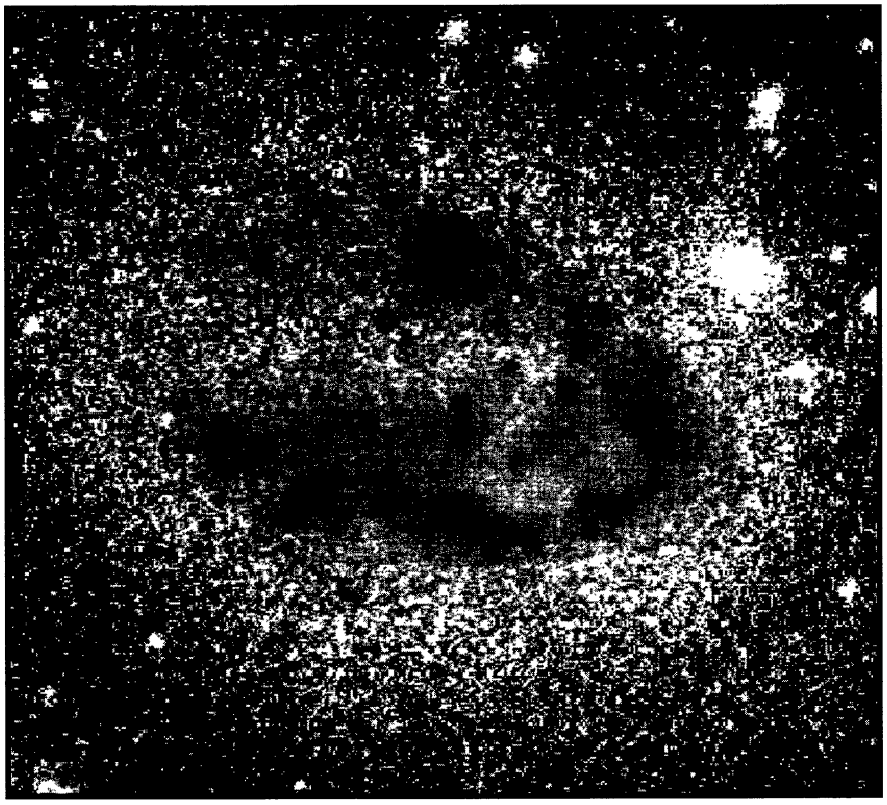

FIG. 2. $C-T_1$ color map of NGC 1427A; darker grey levels correpond to bluer pixels in $C-T_1$. Scale and orientation are the same as in Fig. 1.

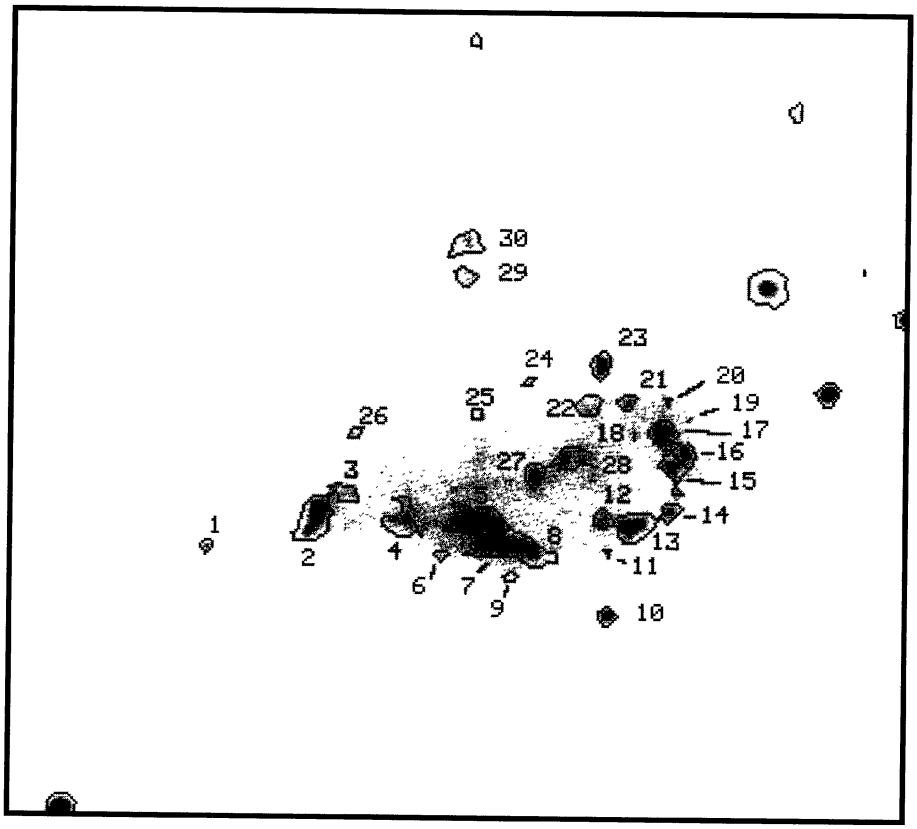

FIG. 3. Greyscale reproduction of the C image, showing HSB regions as contours. The selected blue knots are numbered as in Table 3. Frame size and orientation are the same as for Fig. 1.

guished by their blue colors, confirming the reasonable assumption that they are regions of recent star formation (our spectra show that at least several of them harbor current star forming regions as well, see Sec. *3.3* below). They are seen superposed on a redder underlying stellar population; however, this last population is still quite blue, as can be seen by comparison with the background elliptical galaxy at northwest.

The NO also stands out in the color map. Both the HSB knots and the smooth LSB component of the NO are very blue in $C-T_1$. The faint wisps pointing to the main body of the galaxy are also relatively blue, although hard to see in the color map.

3.3 Photometry and Spectroscopy of the Bright Knots

To isolate the bright blue knots, a high spatial frequency image was constructed in the following way: the C frame was median filtered with a 3×3 pixels window, and then those regions with a large gradient in surface-brightness were identified, creating an image where the low spatial frequencies had been virtually eliminated. We again median filtered this image and clipped all pixels lower than 100 adu (this value corresponds to 3σ of the sky level) to zero and all pixels higher or equal than that value to one, in order to make a mask of the bright, blue regions. Finally, some pixels were interactively put to zero ("by hand") to isolate neighboring regions. We used the C frame because, being this our shortest wavelength passband, the blue knots are best defined.

This mask was used to perform the aperture photometry of the blue knots (see Fig. 3 for their identification). Table 3 lists the measured magnitudes and colors along with their photometric errors. No attempt was made to apply any correction for extinction; Galactic extinction is very low or zero at the latitude of the Fornax Cluster (Burstein & Heiles 1982), and we had no evidence supporting any guess for internal extinction. We prefer to present here the crude colors, since the correction for the underlying red stellar background is rather model-dependant. Next we will consider the mean colors of the background-subtracted knots as a whole to avoid the effects of large errors on individual colors.

With the adopted distance to NGC 1427A, one pixel in our images corresponds to 51 pc. Then, the linear diameters of the selected blue knots range from $\approx$200 pc to nearly 1 kpc, with a median value of 0.5 kpc, indicating that we have probably not been always able to isloate individual complexes of young stars.

Given the lack of observed integrated colors in the Washington system, except for a sample of Milky Way globular clusters (Harris & Canterna 1977), comparison of the observed colors with those of stellar populations of known age and metallicity is performed in a similar way as in CF96: i.e., we used synthetic colors integrated from both theoretical

TABLE 3. Magnitudes and colors of HSB regions.

Number	T_1 mag	$\epsilon_{(T_1)}$ mag	$C-M$ mag	$\epsilon_{(C-M)}$ mag	$M-T_1$ mag	$\epsilon_{(M-T_1)}$ mag
1[a]	19.881	0.019	0.416	0.028	0.551	0.029
2	17.531	0.006	−0.141	0.006	0.351	0.008
3	18.613	0.009	0.120	0.012	0.513	0.014
4	17.609	0.005	0.202	0.007	0.472	0.008
5	16.789	0.003	0.178	0.004	0.474	0.005
6	18.807	0.010	0.192	0.014	0.521	0.015
7	17.083	0.004	0.132	0.005	0.452	0.006
8	18.146	0.007	0.103	0.009	0.492	0.011
9	19.684	0.017	0.263	0.022	0.457	0.025
10[a]	18.215	0.006	0.533	0.010	0.692	0.010
11	20.754	0.028	0.138	0.039	0.549	0.044
12	18.817	0.009	0.138	0.013	0.563	0.014
13	17.603	0.005	0.106	0.007	0.407	0.008
14	19.016	0.012	0.074	0.015	0.474	0.017
15	18.027	0.007	0.143	0.009	0.442	0.010
16	18.739	0.009	0.063	0.012	0.423	0.013
18	20.241	0.018	0.299	0.025	0.511	0.026
19	21.130	0.032	0.212	0.039	0.364	0.045
20	20.119	0.019	0.137	0.025	0.460	0.028
21	18.894	0.010	0.240	0.014	0.493	0.015
22	18.496	0.009	0.189	0.012	0.493	0.013
23	18.610	0.010	0.043	0.011	0.379	0.013
24	20.568	0.030	0.078	0.042	0.579	0.046
25	20.075	0.021	0.190	0.027	0.457	0.031
26	19.831	0.018	0.290	0.023	0.397	0.026
27	18.183	0.006	0.222	0.009	0.547	0.010
28	17.741	0.005	0.294	0.007	0.498	0.008
29	19.438	0.017	−0.136	0.020	0.393	0.025
30	18.862	0.013	−0.224	0.017	0.480	0.020

[a]Foreground star.

TABLE 4. Parameters of model simple stellar populations.[a]

Model	[Fe/H]	t (10^9 yr)	HB morphology	$U-B$ (mag)	$B-V$ (mag)	$C-M$[b] (mag)	$M-T_1$[b] (mag)
SSP1	−2.27	15	blue	−0.02	0.66	0.48	0.59
SSP2	−2.27	15	intermediate	0.01	0.63	0.47	0.57
SSP3	−1.27	15	intermediate	0.09	0.71	0.59	0.63
SSP4	−1.27	15	red	0.10	0.77	0.65	0.67

[a]Buzzoni 1989.
[b]This paper.

TABLE 5. Parameters of observed "template" custers.[a]

Group	[Fe/H]	t (yr)	$U-B$ (mag)	$B-V$ (mag)	$C-M$[b] (mag)	$M-T_1$[b] (mag)
RH II	H II region continuum		−0.98	0.07	−0.47	0.10
Y1	−0.0	10×10^6	−0.65	0.35	−0.14	0.58
Y2	−0.0	50×10^6	−0.25	0.20	0.02	0.31
Y3a[c]	−0.0	100×10^6	−0.12	0.28	0.16	0.33
Y3b	−0.0	100×10^6	−0.07	0.21	0.13	0.22
Y4	−0.0	500×10^6	0.12	0.47	0.43	0.44
I1	−0.0	1×10^9	0.11	0.65	0.54	0.70
I2	−0.0	3×10^9	0.24	0.82	0.78	0.71
G1	+0.0	$>1\times10^{10}$	0.45	0.99	1.02	0.82
G2	−0.5	$>1\times10^{10}$	0.32	0.83	0.84	0.71
G3	−1.0	$>1\times10^{10}$	0.13	0.71	0.64	0.66
G4	−1.5	$>1\times10^{10}$	0.09	0.65	0.56	0.63
G5	−2.0	$>1\times10^{10}$	0.04	0.61	0.50	0.60

[a]Bica 1988.
[b]This paper.
[c]Includes contribution from a group of red giants.

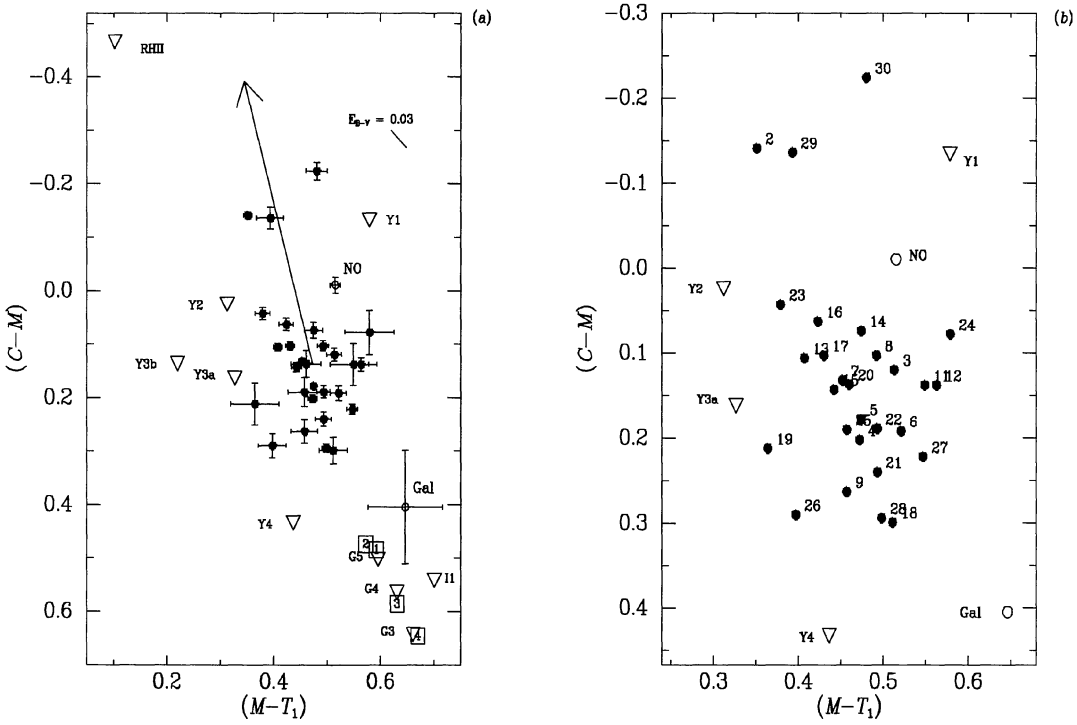

FIG. 4. (a) Two color plot for the blue knots in NGC 1427A (filled circles), backgrounds of galaxy proper and NO (open circles), SSP models (squares), and template spectra (triangles). The arrow connects the median colors of the knots measured before and after background subtraction. (b) Same as (a), except for the scale, and that error bars are not shown. The blue knots are numbered as in Fig. 3.

spectra of simple stellar populations (SSP) and from observed spectra of star clusters.

The former were taken from Buzzoni (1989), and their parameters, along with our calculated Washington colors, are listed in Table 4; the latter are the "template spectra" from the star clusters grid established by Bica & Alloin (1986), and afterwards extended to the near infrared and the ultraviolet spectral regions (Bica & Alloin 1987; Bica *et al.* 1994). Each "template spectrum" corresponds to a group of objects defined in Bica (1988); these groups span a broader range in age than the SSPs do: from $\geqslant 10^{10}$ yr to 10^7 yr, including also an H II region continuum spectrum. Table 5 shows the main properties of these groups, where "Y" stands for "young," "I" for "intermediate," and "G" for "globular cluster–like" populations.

A new calibration of these synthetic colors to the standard system was done via 14 stars with published Washington photometry (Canterna 1976; Harris & Canterna 1979; Geisler 1984; Canterna *et al.* 1986; Geisler *et al.* 1991) and with observed spectral energy distributions; 13 of them were taken from the spectrophotometric atlas of Gunn & Stryker (1983), and the last one from Bohlin *et al.* (1990) and Oke (1990). However, a small difference was noted between the synthetic colors and those of Galactic globular clusters with the corresponding metallicities. As was done in CF96, an empirical correction was applied in the following way: the synthetic colors obtained for the template clusters G1 to G5 were compared with the average colors of the "main objects" of each group listed in Bica *et al.* (1988), deriving the additive corrections $\Delta(C-M) = -0.067$ and $\Delta(M - T_1) = 0.041$. These corrections were then applied to all the integrated colors, either SSPs or template spectra.

Figure 4(a) is a two color plot, where filled circles are the HSB regions, open triangles are the template clusters, and open squares are the SSPs. Open circles are the background colors of the NO and of the main body of NGC 1427A (see below). The same plot is shown in Fig. 4(b), where the scale was changed and the error bars were removed in order to show more clearly the numbers of the HSB regions (labeled as in Fig. 3). Objects #1 and #10 have stellar FWHMs and, judging from their magnitudes and colors (they are the reddest), are most certainly foreground stars; so they were not included in Fig. 4.

The colors of the remaining 28 HSB regions in NGC 1427A scatter along a strip bounded by the colors of Y1 and those of the rest of the young populations (Y2–Y4). Allowing for photometric and possible systematic errors, an important part of this scatter may be due to the different relative contributions from the red background and from nebular emission, and/or differential internal reddening in each region. This last effect is evidenced in that some of the reddest regions (#11, #12, #27, #28, #22, #24) are roughly aligned in a north–south direction, coinciding with a relatively red feature in the color map, possibly a dust lane. A reddening vector for Galactic dust is also shown in Fig. 4(a).

The contribution from the underlying background was estimated from smoothed images where the HSB regions had been eliminated. However, the photometric errors of the

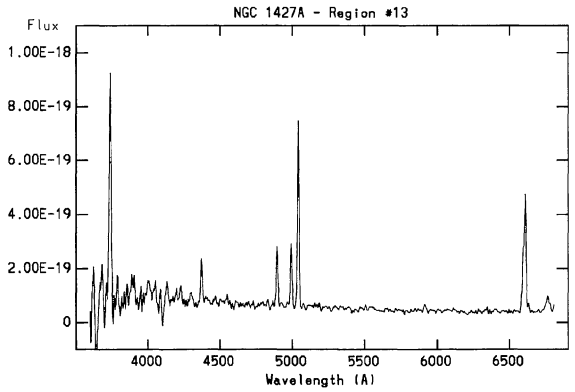

FIG. 5. Spectrum of region #13, boxcar smoothed with a 5 pix (17 Å) wide window. Flux is in units of erg cm^{-2} s^{-1} $Å^{-1}$.

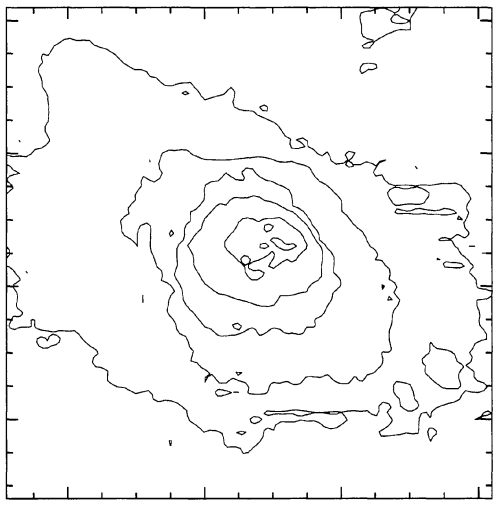

FIG. 6. Contour plot of the north object (C band). The image is 41″ on each side; north is up and east to the left.

HSB regions greatly increase when this background is subtracted, and trying to plot these corrected colors results in a scatter of points with large error bars. So, we plotted in Fig. 4(a) an arrow showing the change in the median colors of the HSB regions after background subtraction. This represents a blueing of 0.53 mag in $C-M$ and 0.13 mag in $M-T1$. The median colors of the backgroud–subtracted HSB regions are then compatible with a young stellar population (group Y1: $t=10^7$ yr) plus a contribution from an H II region continuum (RH II).

The contribution from nebular line emission to the flux within the Washington M and T_1 bands was estimated from the spectra obtained at CASLEO. Figure 5 shows the spectrum of region #13, where features typical for star forming regions can be seen. Regions #2 and #5 show similar spectra, although with weaker emission lines. Within the M band, the emission lines evidently contributing to the total flux are Hβ, and [O III] λλ 4959, 5007; while [N II] λλ 6548, 6584, Hα, and [S II] λλ 6717, 6731 fall within the T_1 passband. The estimated contribution from these lines to the M and T_1 magnitudes are, respectively: 0.03 mag and 0.07 mag for region #2, 0.02 mag and 0.05 mag for region #5, and 0.15 mag and 0.18 mag for region #13. Note that these values could be either underestimations or overestimations, depending on whether the slit coverd a larger or smaller area than the area where we measured the colors. In any case, it is clear that, besides increasing the scatter in both colors, the effect of the nebular emission is a further reddening in $M-T_1$ and also in $C-M$, where the only strong line possibly contributing to the flux within the C band is [O II] λ 3727.

Our data then suggest that the bright knots are in fact younger than 10^7 yr (group Y1), and three out of four or five lying within the spectrograph slit include H II regions. It is then very probable that most of the blue knots harbor regions of current star formation.

A few additional words can be said about the bluest HSB regions. Except for region #2, which is one of the brightest, and hence has a relatively low contribution from the galaxy background, the bluest regions are #29 and #30, those belonging to the NO. Our photometry shows that in this case, their blue colors are not due to bright knots on a red background, but to relatively faint knots on a very faint and blue background. New spectroscopic observations of these knots (recently obtained with the same telescope and instrumental setup described in Sec. 2, but not fully reduced yet) show Hα emission associated with them. The colors of the main body of NGC 1427A, calculated as the median of the colors measured in 13 zones of 5×5 pix between the knots, are $C-M=0.41\pm0.11$ and $M-T_1=0.65\pm0.07$ (point labeled "Gal" in Fig. 4). For the whole NO, we measured $C-M=-0.01\pm0.02$ and $M-T_1=0.52\pm0.02$, using an aperture of 8.4 arcsec (see below) and after subtracting knots #29 and #30 (point labeled "NO" in Fig. 4). This shows that, while the underlying stellar content in NGC 1427A is an intermediately old ($t\lesssim1\times10^9$ yr) population, the NO is almost completely built up by relatively young stars ($t\lesssim5\times10^7$ yr). Alternatively, the main body of the galaxy might be composed by a very metal poor and old population ([Fe/H]$\simeq-2$; $t>10^{10}$ yr). However, metallicity alone cannot be responsible for the blue background of the NO; a young population is needed to reproduce its colors.

3.4 The North Object

In order to study the morphology of the NO we created subimages from the C, M, and T_1 images, centered at this object, where the HSB regions had been removed. These frames were median filtered, and the background contribution from NGC 1427A was subtracted; the result is shown in Fig. 6 for the C subimage, where the roughly circular and concentric isophotes of the NO are clearly seen. We obtained a surface brightness profile for each band by measuring the mean surface brightness within concentric circular isophotes as a function of radius. The C profile is shown in Fig. 7, where the error bars represent the standard deviation within each isophote. Also shown (dashed lines) are the profiles obtained by varying the sky value in ±3.2 adu (the rms of the background fit); it is clear that the error bars are rather pessimistic.

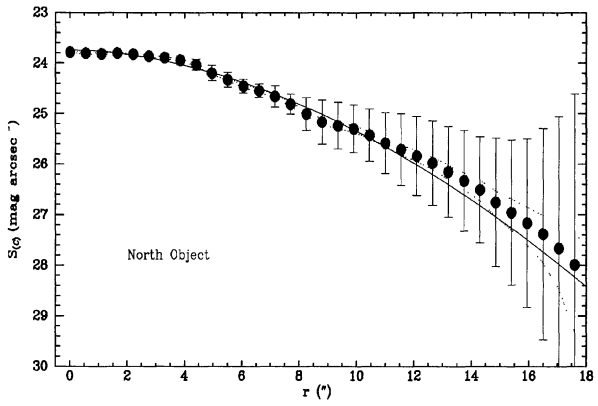

FIG. 7. Surface brightness profile (C band) of the north object; error bars are the standard deviation within each isophote. Dashed lines are the profiles obtained by varying the sky value in ± the rms of the background fit. The continuous line is the fitted model.

Generalized exponential models of the form

$$S_{(r)}=S_0+1.086\left(\frac{r}{\alpha}\right)^N,$$

where S_0 is the central surface brightness, α is the scale parameter, and N is a "shape" parameter, were fitted to each profile. Table 6 lists the parameters obtained from each of the fits, while Fig. 7 shows the fitted model (C image) as a continuous line. The values of α and N for the different bands agree within their respective errors.

Table 7 gives some global properties of the NO obtained from the model parameters: the total T_1 magnitude integrated from the model ($T_{1_{TOT}}$), the radius of the $S_{(T_1)}=26$ mag arcsec^{-2} isophote (r_{26}), and the mean surface brightness within that isophote ($S_{26(T_1)}$). Also given is the absolute blue magnitude, calculated as in Sec. *3.1*.

The structural properties of the NO place it at the faint end of the relations for dE galaxies in the Fornax Cluster as given in Cellone *et al.* (1994). Its luminosity makes it comparable to the fainter dwarfs observed by Bothun *et al.* (1991), which tend to display "flat cores," a feature that mathematically translates into $1<N\leq 2$. In particular, the structural parameters that we obtain for the NO are very close to those measured by Young & Currie (1994, 1995) for the Fornax Cluster dwarf NG 63. This galaxy, although isolated and otherwise inconspicuous, has $B-V=0.48$, a relatively blue color for a dE (Caldwell & Bothun 1987).

Recall that the colors given in Sec. *3.3* (and shown in Fig. 4) were measured without subtracting the contribution from the main body of NGC 1427A. Once this contribution is removed, the colors measured within an aperture equal to the scale length of the profile ($\alpha=8.4$ arcsec) are:

TABLE 6. The North Object: Model parameters.

Band	S_0 (mag arcsec^{-1})	α (arcsec)	N
C	23.74±0.04	8.1±0.3	1.8±0.2
M	23.99±0.04	8.0±0.4	1.9±0.3
T_1	23.70±0.02	8.4±0.4	2.1±0.3

TABLE 7. The North Object: Global properties.

α (kpc)	0.77±0.04
$T_{1_{TOT}}$ (mag)	17.87±0.20
r_{26} (arcsec)	11.9±1.4
r_{26} (kpc)	1.09±0.13
$S_{26(T_1)}$ (mag arcsec^{-1})	24.61±0.11
M_B (mag) [a]	−13.4

[a]Calibration from Geisler (1996).

$C-M=-0.23$ and $M-T_1=0.38$. Although a precise age cannot be derived from these colors alone, it is clear that the NO is composed by young stars, with a very small contribution (if any) from an older population.

When using Geisler's (1996) transformations from Washington to *UBVRI* colors, one should be aware that $U-V$ and $V-I$ indexes are not well reproduced. On the other hand, it is expected that the errors result larger for blue colors ($C-M<0.0$), given the scarcity of blue Washington standard stars used to derive the transformations. A crude estimation of the *UBV* colors of the NO can then be made by comparing its Washington colors with those of the simple stellar populations given in Table 4. A simple interpolation between the colors of groups Y1 and RH II gives $U-B\simeq -0.75$ and $B-V\simeq 0.25$ for the NO. These values are near the blue extreme for dwarf irregular (dI) galaxies, which are known to be bluer than dEs (Gallagher & Hunter 1986), and they are also bluer than the colors of known tidal dwarfs, like the object found at the tip of the southern tail of the "Superantennae" galaxy (Mirabel *et al.* 1991). The colors of the NO are then comparable to colors of blue compact dwarf (BCD) or dI/BCD galaxies, which are undergoing bursts of star formation (Thuan 1985; Drinkwater *et al.* 1996; Krüger & Fritze-v. Alvensleben 1994).

However, without detailed evolutionary models it is not straightforward to affirm how will this object look like when its stellar population gets older, causing its total magnitude and surface brightness to get dimmer.

4. DISCUSSION

From our Washington three-color surface photometry of the irregular galaxy NGC 1427A (along with data from the literature), the following conclusions can be derived.

Regarding its global properties (optical and infrared luminosities and colors, mean surface brightness, H I content) NGC 1427A can be considered a normal irregular galaxy. Its morphology shows a clear assymetry between the southern and northern halves of the galaxy; the former concentrates almost all the HSB regions, while the latter has the appearance of a plume, resembling interacting systems. Alternatively, this feature may just be a spur as sometimes seen in irregular galaxies; in any case, the morphology of NGC 1427A is interesting enough to deserve a kinematical analysis. Detailed optical spectroscopy, as well as a high spatial resolution H I map, wolud be very helpful in this respect.

The HSB regions are not randomly distributed accross the galaxy, but tend to form a "folded ring." Their blue colors are the result of a young population; current star formation is confirmed in several of them through emission lines in their spectra. Different amounts of reddening by local dust, back-

ground contamination, and contribution from nebular emission are responsible for, at least, part of the scatter in their colors; so, it cannot be discarded that the brightest knots (those who best define the distorted ring) have similar intrinsic colors and hence are coeval.

Superposed on the LSB "plume" there is a nearly round object, containing a few HSB regions. This object (the NO) is structurally identical to a faint dE or dI galaxy as those who populate the Fornax Cluster (and other clusters of galaxies as well). Its colors, however, are bluer than those of dEs, and even of most dI galaxies, although they are comparable to the colors of BCDs. Aging of its stars will cause its colors to become redder and its magnitude and surface brightness to become fainter with time; whether this object will look like a faint dwarf spheroidal galaxy within a few 10^8 yr is a matter of discussion.

Without detailed kinematics, although supported by morphological arguments, any association between the NO and the ringlike structure is merely speculative. It is remarkable the similitude between NGC 1427A and interacting systems like Arp 125 and Arp 142, where the main galaxy is distorted and bent towards its spheroidal companion. In particular, the distribution of bright knots in NGC 1427A can be assimilated to an early stage of the model proposed by Freeman & de Vaucouleurs (1974) for the "folded ring" galaxy Arp 144 (see their Fig. 4), although in the present case there is no evidence supporting a model involving the collision between a disk galaxy and an intergalactic gas cloud (and probably neither in Arp 144 itself; see Joy *et al.* 1988, but see also Higdon 1988). It is tempting, however, to explore this scenario, where the NO could be a "tidal dwarf" generated from the debris of the interaction. Note that the absolute magnitude of the NO is within the range for this kind of objects (Hunsberger *et al.* 1996).

Alternatively, instead of being the by–product of an interaction, the NO could be causing it. Numerical simulations show that a close encounter with a low mass companion can induce distortions in the outermost isophotes of a galaxy, resulting in a morphology closely resembling what we see in NGC 1427A. Toomre & Toomre (1972) show the results for models with different mass ratios; lower mass companions take a longer time to develop the distortion (for the same geometrical situation), resulting in configurations where the intruder lies within the bridge of material torn away from the main galaxy, as seems to be the case for the NO. However, no detailed comparison can be made since the mass of the NO is largely uncertain. On the other hand, those simulations start with a differentially rotating disk galaxy as the perturbed object, and this is very probably not true for NGC 1427A, given its Gaussian–shaped H I profile.

Regarding the ring of bright knots, we cannot state whether it existed previously or it was instead generated during the interaction and afterwards distorted. It is known that rings are created in central collisions, while the distortion requires a close passage (see, for example, Binney & Tremaine 1987). Are we seeing then a combination of both processes, or is the morphology of NGC 1427A the result of a process other than an interaction? The photometric data presented in this paper show that the bright knots that form the distorted ring are younger than 10^7 yr; taking this as a plausible age for the ring, and 5 kpc as the projected distance from the NO to the center of the ring, a crude estimate of the projected relative velocity of the NO can be set at $\simeq$500 km/sec, or 150% of the velocity dispersion of the Fornax Cluster (see Sec. 1). We have not at this stage the sufficient data to answer the previous questions; it is plausible that a strong dynamical process may be responsible for the peculiar morphology of NGC 1427A, and it is clear that the NO is a structurally distinct object which should be taken into account as playing an important role in this scenario.

The authors acknowledge use of the CCD and data acquisition system supported under U. S. National Science Foundation grant AST-90-15827 to R. M. Rich. We are also indebted to R. Barbá for his help with the reduction of the spectroscopic observations, and to an anonymous referee for helpful suggestions. S.A.C. wishes to thank CASLEO staff members J. L. Giuliani and A. De Franceschi, along with their respective wives and children, for a delightful New Year day spent at the mountain.

REFERENCES

Aaronson, M., Dawe, J. A., Dickens, R. J., Mould, J. R., & Murray, J. B. 1981, MNRAS, 195, 1P
Arp, H. 1966, ApJS, 14, 1
Baldwin, J. A., & Stone, R. P. S. 1984, MNRAS, 206, 241
Bica, E. 1988, A&A, 195, 76
Bica, E., & Alloin, D. 1986, A&A, 162, 21
Bica, E., & Alloin, D. 1987, A&A, 186, 49
Bica, E., Alloin, D., & Schmitt, H. R. 1988, A&A, 202, 8
Bica, E., Alloin, D., & Schmitt, H. R. 1994, A&A, 283, 805
Binney, J., & Tremaine, S. 1987, Galactic Dynamics (Princeton University Press, New Jersey)
Bohlin, R. C., Harris, A. W., Holm, A. V., & Gry, C. 1990, ApJS, 73, 413
Bothun, G. D., Caldwell, N., & Schombert, J. M. 1989, AJ, 98, 1542
Bothun, G. D., Impey, C. D., & Malin, D. F. 1991, ApJ, 376, 404
Bureau, M., Mould, J. R., & Staveley-Smith, L. 1996, ApJ, 463, 60
Burstein, D., & Heiles, C. 1982, AJ, 87, 1165
Buzzoni, A. 1989, ApJS, 71, 817
Caldwell, N., & Bothun, G. D. 1987, AJ, 94, 1126
Canterna, R. 1976, AJ, 81, 228
Canterna, R., Geisler, D., Harris, H. C., Olszewski, E., & Schommer, R. 1986, AJ, 92, 79
Cellone, S. A., & Forte, J. C. 1996, ApJ, 461, 176 (CF96)
Cellone, S. A., Forte, J. C., & Geisler, D. 1994, ApJS, 93, 397
de Jong, T., Clegg, P. E., Soifer, B. T., Rowan-Robinson, M., Habing, H. J., Houck, J. R., Aumann, H. H., & Raimond, E. 1984, ApJ, 278, L67
de Vaucouleurs, G., de Vaucouleurs, A., & Corwin, H. G. 1976, Second Reference Catalogue of Bright Galaxies (University of Texas Press, Austin)
Drinkwater, M. J., Currie, M. J., Young, C. K., Hardy, E., & Yearsley, J. M. 1996, MNRAS, 279, 595
Feitzinger, J. V., & Galinski, Th. 1985, A&AS, 61, 503
Ferguson, H. C. 1989, AJ, 98, 367
Ferguson, H. C., & Sandage, A. 1990, AJ, 100, 1
Freeman, K. C., & de Vaucouleurs, G. 1974, ApJ, 194, 569
Gallagher, J. S., & Hunter, D. A. 1984, ARA&A, 22, 37
Gallagher, J. S., & Hunter, D. A. 1986, AJ, 92, 557

Geisler, D. 1984, PASP, 96, 723
Geisler, D. 1990, PASP, 102, 344
Geisler, D. 1996, AJ, 111, 480
Geisler, D., Clariá, J. J., & Minniti, D. 1991, AJ, 102, 1836
Geisler, D., & Forte, J. C. 1990, ApJ, 350, L5
Gunn, J. E., & Stryker, L. L. 1983, ApJS, 52, 121
Harris, H. C., & Canterna, R. 1977, AJ, 82, 798
Harris, H. C., & Canterna, R. 1979, AJ, 84, 1750
Higdon, J. L. 1988, ApJ, 326, 146
Hunsberger, S. D., Charlton, J. C., & Zaritsky, D. 1996, ApJ, 462, 50
Hunter, D. A., & Gallagher, J. S. 1985, ApJS, 58, 533
Hunter, D. A., Gillet, F. C., Gallagher, J. S., Rice, W. L., & Low, F. J. 1986, ApJ, 303, 171
Isserstedt, J., & Schindler, R. 1986, A&A, 167, 11
Jones, J. E., & Jones, B. J. T. 1980, MNRAS, 191, 685
Joy, M., Ellis, Jr., H. B., Tollestrup, E. V., Brock, D., Higdon, J. L., & Harvey, P. M. 1988, ApJ, 330, L39
Kennicutt, R. C., Keel, W. C., van der Hulst, J. M., Hummel, E., & Roettiger, K. A. 1987, AJ, 93, 1011
Krüger, H., & Fritze-v. Alvensleben, U. 1994, A&A, 284, 793
Laustsen, S., Madsen, C., & West, R. M. 1987, A la Decouverte du Ciel Austral (Springer, Berlin)
Mirabel, I. F., Lutz, D., & Maza, J. 1991, A&A, 243, 3697
Oke, J. B. 1990, AJ, 99, 1621
Ostrov, P., Geisler, D., & Forte, J. C. 1993, AJ, 105, 1762
Reif, H., Mebold, U., Goss, W., van Woerden, H., & Seigman, B. 1982, A&AS, 50, 451
Soifer, B. T., Houck, J. R., & Neugebauer, G. 1987, ARA&A, 25, 187
Sprayberry, D., Impey, C. D., Bothun, G. D., & Irwin, M. J. 1995, AJ, 109, 558
Tammann, G. 1980, in ESO/ESA Workshop on Dwarf Galaxies, edited by M. Tarenghi and K. Kjär (ESO/ESA, Geneva), p. 3
Thuan, T. X. 1985, ApJ, 299, 881
Toomre, A., & Toomre, J. 1972, ApJ, 178, 623
van den Bergh, S. 1989, ARA&A, 1, 111
Young, K. C., & Currie, M. J. 1994, MNRAS, 268, L11
Young, K. C., & Currie, M. J. 1995, MNRAS, 273, 1141